

Evaluation of Optimal Yaw Rate Reference for Electric Vehicle Torque Vectoring

E.N. Smith, E. Velenis & D. Cao
Advanced Vehicle Engineering Centre
Cranfield University, Bedford, UK

D. Tavernini
Centre for Automotive Engineering
University of Surrey, Guildford, UK

Published by CRC Press. This is the Author Accepted Manuscript. This article may be used for personal use only.

The final published version (version of record) is available online at DOI:10.1201/9781315265285. Please refer to any applicable publisher terms of use.

ABSTRACT: This work evaluates the intrinsic contribution of the yaw rate reference to the overall handling performance of an electric vehicle with torque vectoring in terms of minimum-time manoeuvring. A ‘Time-Optimal’ Yaw rate reference (TOY) derived from optimal control problems was generated which coincides exactly with the analytical steady-state single-track expression for yaw rate gain. Alternative yaw rate references are compared with TOY through closed-loop optimal control simulations. Results show that when yaw rate reference, parameterised by understeer gradient, is set away from the ‘time-optimal’ value, performance is degraded at a rate of 0.65s/deg/g.

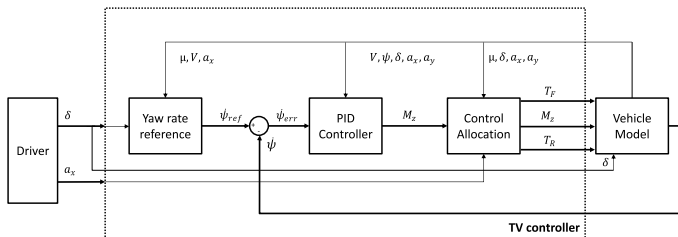


Figure 1: Torque vectoring controller schematic

1 INTRODUCTION

Active yaw control systems for improved performance and safety have been commonplace on passenger vehicles for the past two decades. Modern all-wheel-drive electrified vehicles (EVs) offer substantial opportunities for active control of yaw dynamics by over-actuation, namely torque vectoring (TV); the distribution of wheel torques between multiple wheels. TV extends the maximum cornering force by superior distribution of yaw moment, making better use of friction availability [1].

With reference to Figure 1, TV systems typically follow a yaw rate reference, achieved by tuning of a Controller and a subsequent Control Allocation (CA) for torque arbitration between individual wheels. Advanced techniques using mathematical analysis and simulation tools have been used to optimise both controller [2] and CA [3, 4] performance, yet very little

rigorous work has been undertaken into research of the optimal yaw rate reference. The majority of yaw rate references have been derived from the steady-state single-track linear-tyre equations, modifying the handling for stability or agility by selecting an appropriate understeer gradient, K .

De Novellis et al. [3] chose a reference heuristically between achievable limits on the dynamic steer-lateral acceleration ‘handling diagram’, such that responsiveness is maximised in the linear region, the linear region is extended and lateral acceleration boundary maximised. Limits are calculated by steady-state analysis of a single-track model with nonlinear tyres, taking into account a direct yaw moment term. Wheals et. al. [5] constructed a yaw rate map by interrogation of a high-fidelity model at steady-state considering equal wheel torques, and noted significant differences to the single-track model map attributed to roll and nonlinear tyres. This was not trialled within a controller; they went on to use a linearised two-track model considering nonlinear tyres and aerodynamic forces in which sideslip and velocity derivatives are decoupled and the reference set presuming zero sideslip and no longitudinal acceleration. No evaluation of the reference *per se* was made.

A first-order delay to account for the yaw inertia of the vehicle has been incorporated by [5, 6], however Bünthe et. al. [7] proposed a yaw rate reference considering fully-dynamic elements, combining steady-

state and lateral dynamics transfer functions from the single-track model, tuned heuristically to modify the transient response.

The aim of this research is to evaluate the contribution of the yaw rate reference to overall vehicle performance within a closed-loop TV control system. This work presents ‘TOY’, a mathematically ‘Time-Optimal’ Yaw rate reference for an electric sportscar with 4-wheel torque vectoring capability. The performance of TOY over a U-turn manoeuvre is then compared against two K -parameterised references.

2 VEHICLE SYSTEM MODELLING

This study uses a three degree of freedom single-track model with linear tyres (equations (1-3)), parameterised to represent a high-performance EV with an electric motor powering each wheel independently. To emulate left-right torque vectoring, a direct yaw moment, M_z , is included in the yaw acceleration equation (3). Lateral load transfer is neglected, along with roll and pitch dynamics.

$$m\dot{V}_x = m(a_x + V_y\dot{\psi}) \quad (1)$$

$$m\dot{V}_y = -\frac{C_f C_r}{V_x} V_y + \left(-mV_x + \frac{(-l_f C_f + l_r C_r)}{V_x}\right) \dot{\psi} + C_f \delta \quad (2)$$

$$I_z \ddot{\psi} = -\frac{(l_f C_f + l_r C_r)}{V_x} V_y - \frac{(l_f^2 C_f + l_r^2 C_r)}{V_x} \dot{\psi} + l_f C_f \delta + M_z \quad (3)$$

where a_x is the longitudinal acceleration, considered as an input to the system, m is the vehicle mass; $\dot{\psi}$ is the yaw rate; I_z is the yaw moment of inertia about the vertical axis; l_f and l_r are the distances of the front and rear axles to the centre of gravity (CG); C_f and C_r are the front and rear tyre cornering stiffnesses; V_x and V_y are the longitudinal and lateral vehicle velocities respectively. Retarding torque is provided exclusively by regenerative braking.

A linear tyre model with cornering stiffness dependent on normal load is used, considering a quasi-steady-state approximation to normal load.

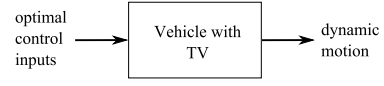
$$F_{yj} = -C_j \alpha_j = -\eta_j F_{zj} \alpha_j \quad (4)$$

$$\text{where } C_j = \eta_j F_{zj} \quad (5)$$

$$F_{zf} = \frac{mg l_r}{L} - \frac{h}{L} m a_x, \quad F_{zr} = \frac{mg l_f}{L} + \frac{h}{L} m a_x \quad (6)$$

where for each $j \in [f, r]$, η_j is the tyre cornering coefficient, α_j is the tyre slip angle, F_{zj} is the axle normal load and F_{yj} is the axle lateral force on front and

a) Open-loop control method



b) Closed-loop control algorithm

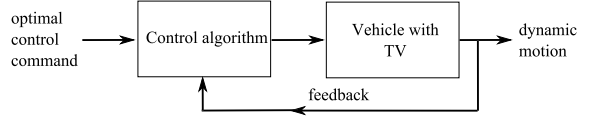


Figure 2: Open-loop control method and closed-loop control algorithm after [9]

rear. g is the gravitational acceleration constant, L is the wheelbase, h is the height of the CG. The natural (uncontrolled), steady-state understeer gradient of the vehicle is defined as [8]:

$$K_{nat}^{SS} = \left(\frac{1}{\eta_f} - \frac{1}{\eta_r} \right) / g, \quad (7)$$

and modified by selecting cornering coefficient values η_f and η_r , assuming that the cornering coefficient is constant. A 50:50 static distribution is used for the vehicle without TV control. For TV, front-rear torque vectoring is modelled by distributing torques front-rear by a CA that allocates longitudinal forces in proportion to the normal load on the axle (8), found to be the optimal distribution [4]:

$$F_{xj} = m a_x \frac{F_{zj}}{F_{zf} + F_{zr}}. \quad (8)$$

Neglecting wheel spin axis rotational inertia, wheel torques become

$$T_{xj} = F_{xj} R_w, \quad (9)$$

where R_w is the rolling radius of the tyres. Longitudinal and lateral forces are coupled and saturated at the limit by friction circle constraints (10):

$$\left(\frac{F_{xj}}{F_j} \right)^2 + \left(\frac{F_{yj}}{F_j} \right)^2 \leq \bar{\mu}_{max}^2, \quad (10)$$

$$\text{where } F_j = \bar{\mu} F_{zj}, \quad (11)$$

with $\bar{\mu}$ is tyre-road friction coefficient.

3 OPTIMAL CONTROL FORMULATIONS

To determine the ‘time-optimal’ yaw rate reference and hence evaluate it within a TV control system, two different optimal control problem (OCP) formulations are required, as shown in Figure 2. Figure 2a shows the *open-loop control method* (after [9]), which permits the maximum performance potential of TV to be determined, considering optimal control inputs from a ‘perfect’ driver, including M_z , applied to the vehicle directly and is used to generate the

‘Time-optimal’ yaw rate reference in section 4. In reality optimal open-loop control defined in this way is unrealisable in the real world. Figure 1 shows a TV control system that determines torques that must be applied at each wheel, via a controller, from a desired yaw rate reference. As shown in figure 2b, this is defined as a *closed-loop control algorithm*. This *closed-loop control algorithm* is incorporated into an OCP in section 5 to evaluate the relative performance of different yaw rate references. The optimal control problems may be mathematically formulated as follows. Consider a dynamic system in the form:

$$\dot{\mathbf{x}} = \mathbf{f}[\mathbf{x}(t), \mathbf{u}(t)]; \quad (12)$$

subject to initial and final conditions:

$$\mathbf{x}(t_0) = \mathbf{x}_0, \quad \mathbf{x}(t_f) = \mathbf{x}_f. \quad (13)$$

An OCP seeks to find the control vector sequence \mathbf{u} to minimise a certain cost function, subject to equality and inequality constraints:

$$J = \phi[\mathbf{x}(t_f)] + \int_{t_0}^{t_f} L[\mathbf{x}(t), \mathbf{u}(t)], \quad (14)$$

$$\mathbf{p}[\mathbf{x}(t), \mathbf{u}(t)] = 0, \quad \mathbf{g}[\mathbf{x}(t), \mathbf{u}(t)] \leq 0. \quad (15)$$

Road boundary constraints are simplified by a change of coordinate reference frame from vehicle-centred to road-centred ‘curvilinear’ coordinates:

$$w_{R,l} \leq s_n \leq w_{R,r}, \quad (16)$$

where $w_{R,l}$ and $w_{R,r}$ denote the left and right road widths. By changing the independent variable from time to distance travelled along the road centreline, s , vehicle dynamics may be expressed in terms of lateral position, s_n , and the angle of the vehicle, χ , relative to the road centreline. Dynamic system equations (12)-(15) are transformed from a time-base to s as follows:

$$\frac{dx}{ds} = x' = \frac{dx}{dt} \frac{dt}{ds} = \dot{x} \dot{s}^{-1}, \quad (17)$$

where x is any state variable. Other constraints include steering control bandwidth (limited to 1Hz), imposition of a maximum steer angle and motor power/torques constrained according to a power curve:

$$|\delta| \leq \delta_{max}, \quad |\dot{\delta}| \leq \dot{\delta}_{max}, \quad (18)$$

$$F_{xj} V_x \leq P_{max,j}, \quad (19)$$

where $P_{max,j}$ is the maximum power of the motors. To seek to minimise time of travel, the cost function becomes:

$$J(t) = \int_{t_0}^{t_f} dt \quad \mapsto \quad J(s) = \int_{s_0}^{s_f} \frac{1}{\dot{s}} ds. \quad (20)$$

The state and control vectors are

$$\mathbf{x} = \{V_x, V_y, \psi, x_R, y_R, \theta_R, s_n, \chi, \delta, t\}^T, \quad (21)$$

$$\mathbf{u} = \{a_x, \dot{\delta}\}^T, \quad (22)$$

where x_R , y_R & θ_R are position and heading of the road centreline respectively, t is elapsed time. For the *Open-loop control method* (TV active), the control vector includes yaw moment: $\mathbf{u} = \{a_x, M_z, \dot{\delta}\}^T$. *GPOPS-II* [10], was used to transcribe the continuous-time OCP into a discrete non-linear programming problem (NLP), and solved using sequential quadratic programming.

4 OPEN-LOOP CONTROL

This section will determine the *open-loop control method* performance used to identify the ‘time-optimal’ yaw rate reference that the closed-loop TV controller should follow. A left-hand U-Turn manoeuvre consisting of two 30m straights joined by a bend of tightening radius of curvature, up to an apex radius of 35m is used. Straight-line running conditions were enforced at the start of the manoeuvre. Figure 3 overlays states, controls and calculated quantities for the vehicle with TV active (*TV*) and TV inactive (*Unctrl*).

Manoeuvre time is 0.374s faster with *TV* than *Unctrl*. This is a significant time improvement for just one corner, and shows the performance of the 4-motor topology. With reference to figures 3a & 3g, it is clear that *TV* is able to sustain a greater level of drive/brake torque and hence can both start and exit the manoeuvre at higher speeds. *Unctrl* is able to maintain higher speed over $s \in [90, 120]$ and thus gains time back during this portion of the manoeuvre. It exhibits steady-state behaviour here; maintaining constant yaw rate, sideslip and vehicle speed. *TV* is able to accelerate and brake much more aggressively than *Unctrl*, which is forced to coast during the constant radius section.

A dynamic scenario is considered, yet the steady-state (instantaneous) understeer gradient is still useful in giving an indication of vehicle handling behaviour, defined as follows:

$$K_{inst}^{SS} = \frac{\frac{V\delta}{\psi} - L}{V^2}. \quad (23)$$

K_{inst}^{SS} is plotted in figure 3e: the key finding is that *TV* is able to achieve the natural steady-state understeer gradient, K_{nat}^{SS} , throughout the manoeuvre whereas *Unctrl* handling exhibits oversteer relative to K_{nat}^{SS} under braking and understeer relative to K_{nat}^{SS} during acceleration, an effect well-known due to longitudinal load transfer effects.

Friction utilisation is defined as the axle lateral/longitudinal or total force divided by the axle normal load and plotted in figures 3d (front) & 3i (rear). Examination of slip angles in figure 3j is another use-

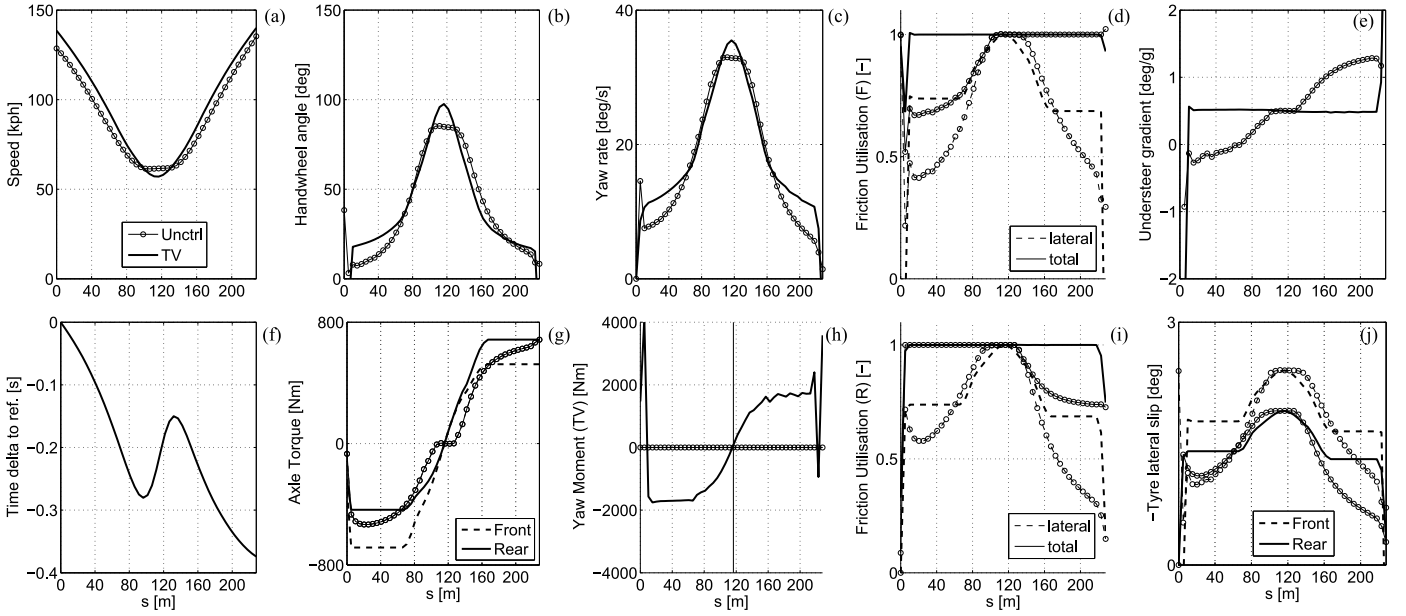


Figure 3: Comparison of *Open-loop control method*: TV inactive (*Unctrl*) (o) against TV active (TV)(no marker)

ful tool for understanding the dynamic handling balance. It is useful also to consider how understeer gradient is related to slip angles [8]:

$$K_{inst}^{SS} = (\alpha_f - \alpha_r)/a_y. \quad (24)$$

Referring to figures 3i & 3j, under braking, *Unctrl* has a reduced rear lateral friction capability due to longitudinal load transfer. Hence α_r is increased and α_f reduced, resulting in a oversteer balance relative to K_{nat}^{SS} (0.5deg/g). The opposite is true during acceleration. *TV* yaw moment, M_z , shown in figure 3h, is stabilising under braking and destabilising during acceleration in order to counteract load transfer effects and achieve a constant K_{inst}^{SS} equal to K_{nat}^{SS} . Figure 4 shows how yaw moment affects lateral force and slip angle for the left turn. Under braking (fig. 4a), stabilising M_z is applied clockwise, such that larger lateral force from the front tyres can be applied in the direction of the turn to maintain yaw dynamic equilibrium. As a result, figures 3j,d,i & e respectively show larger front slip angles are developed, tyre friction availability maximised, and K_{inst}^{SS} exhibits a greater degree of understeer with respect to *Unctrl*. Figure 4b shows the acceleration case. Figure 3j shows that *Unctrl* develops larger slip angles at the front than rear due to load transfer (understeer relative to K_{nat}^{SS}). *TV*, however, is able to develop greater slip angle at the rear than *Unctrl* to balance the destabilising yaw moment and hence make full use of the friction available, counteracting the tendency to understeer. Observation of figure 3h shows that magnitude of yaw moment is proportional to a_x . This trend of direct yaw control effecting a stabilising yaw moment under deceleration and a destabilising yaw moment under acceleration is confirmed by [4] for a similar topology and by [3] where a non-linear yaw rate reference independent of a_x is used.

A ‘time-optimal’ yaw rate reference was derived

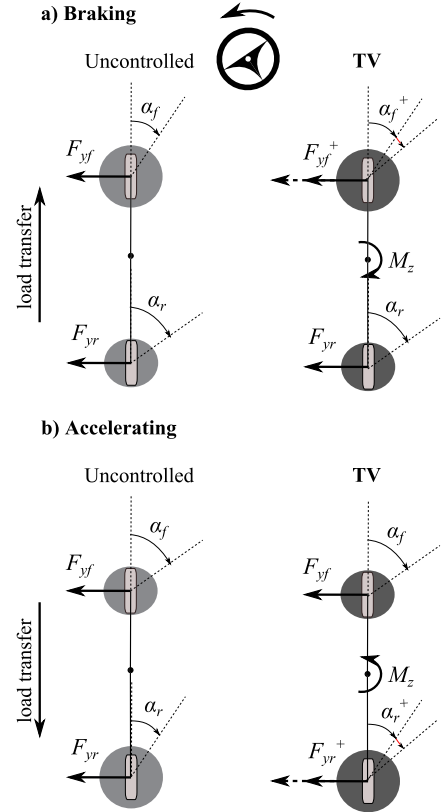


Figure 4: Analysis: TV yaw moment effect on lateral force potential and slip angles and therefore understeer gradient

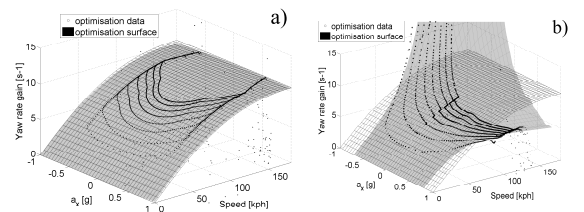


Figure 5: Yaw rate gain surfaces as a function of speed and longitudinal acceleration dynamic OCP results (grey surface) overlaid on steady-state analytic (mesh) for a) TV and b) uncontrolled.

from analysis of the OCPs described, repeated for U-turns with turn radius $R \in [10:10:80]\text{m}$. Figure 5 shows yaw rate gain as a function of longitudinal acceleration and speed for *TV* and *Unctrl*. The grey surface are the results from optimisations and the mesh is the steady-state analytical definition [8]:

$$\frac{\dot{\psi}}{\delta} = \frac{V}{K_{nat}^{SS}V^2 + L}, \quad (25)$$

Figure 5b shows the *Unctrl* result. Under braking, yaw rate gain oversteers the natural characteristic (yaw rate gain tending to infinity at critical speed); under acceleration the yaw rate gain tends towards an understeer response. Where $a_x=0\text{m/s}^2$, the numerical fit from OCPs intersects the analytical solution. Figure 5b generalises the specific solution for *TV*: that for all dynamic manoeuvres in this range, *TV* is able to negate load transfer effects such that the yaw rate gain response is identical to the steady-state response. Therefore, the analytical definition is adopted as the benchmark ‘Time-Optimal’ Yaw rate reference (TOY) against which to compare other references.

5 CLOSED-LOOP CONTROL

This section includes closed-loop control in the OCP to determine the relative performance of references: the major contribution of this work. Small modifications are made to the optimal control formulation used to generate the TOY in section 4. The OCP is now used to find the optimal control history of a ‘perfect’ driver’s steering and accelerator/brake inputs. Figure 1 shows this OCP formulation. It consists of a simplified TV controller (based on an experimentally-validated version [6]) which converts the driver inputs and vehicle states into a reference yaw rate. Yaw moment demand, M_z is output by a PID controller with yaw rate error input. Recall (8) for the CA.

The ability of this *closed-loop control algorithm* to convert the theoretical maximum performance into actuality may be determined. Three variations of the steady-state single-track yaw rate reference—where K_{nat}^{SS} is replaced by K_{tar} in (25)—are compared by setting the TOY reference $K_{tar} = K_{nat}^{SS} = 0.5\text{deg/g}$ and then $K_{tar} = K_{nat}^{SS} \pm 0.5\text{deg/g}$, i.e. $K = K_{tar} \in [0 : 0.5 : 1.0]\text{deg/g}$.

Table 1: Effect of yaw rate target (TV), $K_{nat}^{SS} = 0.5\text{deg/g}$

Simulation	K_{tar} (deg/g)	Time (s)	Δt (s)
OL Baseline	n/a	8.8269	-0.0176
CL $K_{nat}^{SS}+0.5$	+1.0	9.1597	+0.3152
CL K_{nat}^{SS} (TOY)	+0.5	8.8445	+0.0000
CL $K_{nat}^{SS}-0.5$	+0.0	9.1974	+0.3529

Referring to Table 1, the closed-loop (CL) controller including the TOY as reference is 0.0176s

slower than the open-loop (OL) baseline. Since the controller is well tuned for a realistic real-world implementation and the CA is a good compromise between optimality and simplicity for practical implementation, these elements are not modified and therefore all differences in performance between CL optimisations will be a result of the contribution of the yaw rate reference only. Inspection of the time deltas, Δt , reveals approximately equal time loss of $\sim 0.3\text{s}$ for both comparison references, the mean rate of time loss is 0.67s/deg/g as K_{tar} moves away from TOY (K_{nat}^{SS}), 7.5% of the TOY manoeuvre time. This is a clear demonstration not only that the optimal yaw rate reference should follow the natural, uncontrolled, steady-state behaviour of the vehicle but that selection of a sub-optimal yaw rate reference has a highly negative effect on manoeuvre time and therefore the selection of the reference is crucial. Figure 6 overlays states, controls and calculated quantities for the CL results for each yaw rate reference. In figure 6h, TOY ($K_{tar} = 0.5\text{deg/g}$) yaw moment transitions from stabilising under braking to destabilising under acceleration to overcome load transfer effects, as in section 4. Figure 6a shows that TOY achieves highest minimum speed by some margin, which corresponds, in figure 6f, with the greatest change in Δt during $s \in [90, 140]\text{m}$, at which point, in figure 6c, the difference in yaw rate is greatest. TOY achieves the highest yaw rate and correspondingly, the lowest manoeuvre time. Figures 6d,i & figure j plot front and rear friction utilisation and tyre lateral slip respectively. The comparison reference cannot match TOY due to a reduction in total friction utilisation at the unsaturated tyre. Taking the $K_{tar} = 0\text{deg/g}$ case as an exemplar, in figure 6d, front friction utilisation drops from 80% under maximum braking to a 60% minimum at the apex, at which point lateral friction utilisation increases. Total utilisation decreases since longitudinal acceleration reduces to zero. Overall friction utilisation cannot be increased, since front friction utilisation cannot be increased. This would require an increase in front lateral force and therefore slip angle and hence alter the balance too far towards understeer, away from the target $K_{tar} = 0\text{deg/g}$ balance. The total friction capability and therefore performance, then, is limited by K_{tar} , which requires a certain difference between front and rear slip angles which in turn dictates the permissible lateral force at front or rear. Only by following TOY ($K_{tar} = 0.5\text{deg/g}$) can friction be fully utilised and manoeuvre time minimised.

6 CONCLUSIONS

This work found that the ‘Time-Optimal’ Yaw rate reference (TOY) derived from optimal control for a sportscar with 4-wheel independent torque vectoring coincides exactly with the analytical steady-state single-track expression for yaw rate gain. The unique contribution of this research was the inclu-

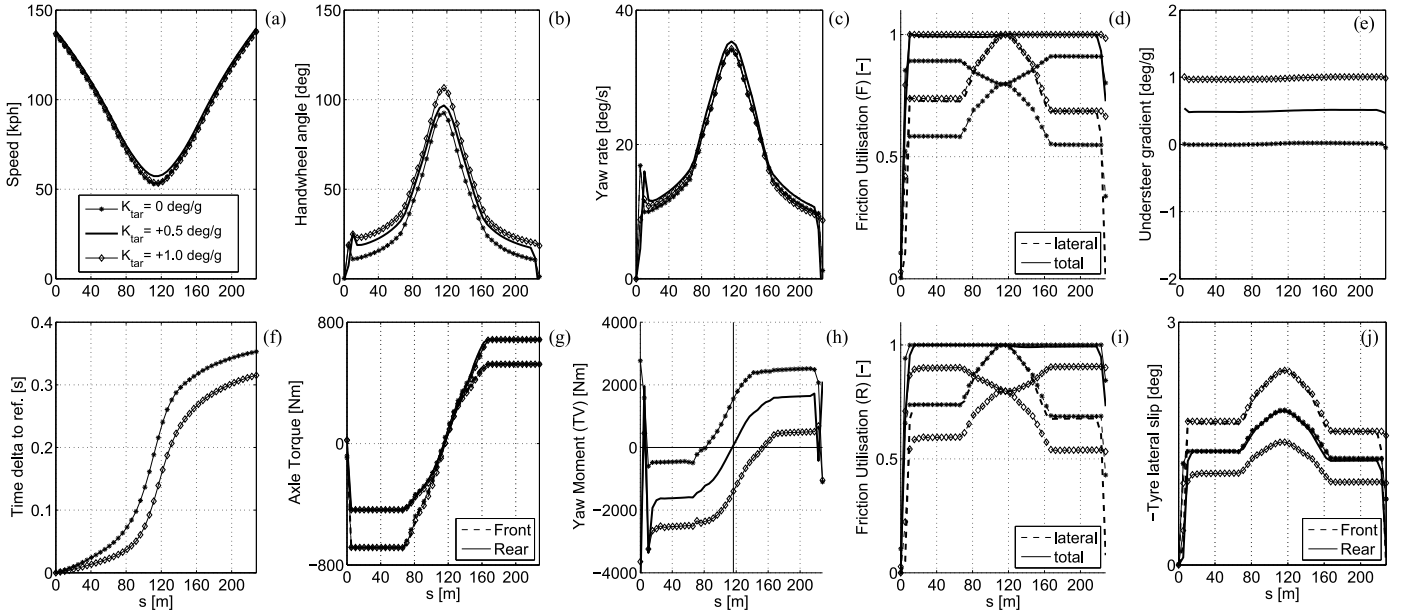


Figure 6: *Closed-loop control algorithm: comparison of yaw rate reference. 0deg/g (*), TOY 0.5deg/g (no marker), 1deg/g (◇)*

sion of a closed-loop controller within an optimal control problem; results found that setting yaw rate reference away from natural understeer gradient degrades performance at a rate of 0.65s/deg/g, which equates to 7.3%/deg/g of the TOY manoeuvre time. TOY achieves the highest minimum speed of the references compared and the greatest yaw rate. TOY is able to use all the available friction at all times by optimising front and rear lateral forces. This study has contributed a rational, mathematical approach to determining optimal yaw rate references and a method by which to objectively compare yaw rate reference performance.

FUNDING

The lead author gratefully acknowledges the support of an ESPRC iCASE industrial studentship with Jaguar Land Rover.

REFERENCES

- [1] Crolla DA, Cao D. The impact of hybrid and electric powertrains on vehicle dynamics, control systems and energy regeneration. *VSD*. 2012 Jan;50(sup1):95–109.
- [2] Siampis E, Velenis E, Longo S. Rear wheel torque vectoring model predictive control with velocity regulation for electric vehicles. *VSD*. 2015;53(11):1555–1579.
- [3] De Novellis L, Sorniotti A, Gruber P. Wheel torque distribution criteria for electric vehicles with torque-vectoring differentials. *IEEE Transactions on Vehicular Technology*. 2014; 63(4):1593–1602.
- [4] de Castro R, Tanelli M, Araujo RE, Savaresi SM. Minimum-time manoeuvring in electric vehicles with four wheel-individual-motors. *VSD*. 2014 Jun;52(6):824–846.
- [5] Wheals JC, Baker H, Ramsey K, Turner W. Torque vectoring AWD driveline: Design, simulation, capabilities and control. 2004; SAE Technical Paper 2004-01-0863.
- [6] Smith E, Tavernini D, Claret C, Velenis E, Cao D. Optimal yaw-rate target for electric vehicle torque vectoring system. In: *IAVSD 2015, Graz*. CRC Press; 2016. p. 107.
- [7] Bunte T, Kaspar S, Hohmann S, Brembeck J. Inverse model based torque vectoring control for a rear wheel driven battery electric vehicle. In: *IFAC World Congress*; 2014.
- [8] Wong JY. *Theory of ground vehicles*. John Wiley & Sons; 2001.
- [9] Horiuchi S. Evaluation of chassis control algorithms using controllability region analysis. In: *IAVSD 2015, Graz*. CRC Press; 2016. p. 35.
- [10] Patterson MA, Rao AV. Gpops-II: A matlab software for solving multiple-phase optimal control problems using hp-adaptive gaussian quadrature collocation methods and sparse nonlinear programming. *ACM TOMS*. 2013;39(3):1–41.